Results in Engineering 23 (2024) 102723

Contents lists available at ScienceDirect

Results in Engineering

journal homepage: www.sciencedirect.com/journal/results-in-engineering

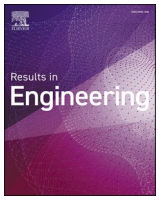

Explainable ensemble learning framework for estimating corrosion rate in suspension bridge main cables

Alejandro Jimenez Rios [a], Mohamed El Amine Ben Seghier [a,*], Vagelis Plevris [b], Jian Dai [a]

[a] Department of Built Environment, Oslo Metropolitan University, Oslo, Norway
[b] Department of Civil and Environmental Engineering, Qatar University, Doha, Qatar

ARTICLE INFO

Keywords:
Suspension bridges
Main cables
Annual corrosion rate
Ensemble learning models
Regression techniques
Shapley additive explanations

ABSTRACT

Ensuring the safe operation of suspension bridges is paramount to prevent unwanted events that can cause failures. Therefore, it is crucial to continuously monitor their operational status to uphold safety and reliability levels. However, natural deterioration caused by the surrounding environment, primarily due to corrosion, inevitably impacts these structures over time, particularly the main cables made of steel. In this study, a robust framework is proposed to predict the annual corrosion rate in main cables of suspension bridges, while investigating the impact of the surrounding environmental factors on this process. To do so, the implementation of four regression models and four machine learning techniques are used in the first phase for modeling the annual corrosion rate based on a comprehensive database containing various environmental factors. The modeling performance is evaluated through a range of statistical and graphical metrics. After that, Shapley Additive Explanations (SHAP) is utilized to explain the model and to extract the impact of each variable on the final modeling results. Overall, the findings demonstrate the effectiveness of the proposed framework for addressing this issue. The Extreme Gradient Boosting (XGB) emerged as the top-performing model, achieving an overall R^2 of 0.982. Moreover, the SHAP findings highlight the impact of CL^- on the annual corrosion rate as the factor with the highest influence during the modeling process. The high performance of the proposed model suggests its potential utility in further research concerning the reliability of suspension bridge main cables.

1. Introduction

Bridges represent key assets in transportation networks as they enhance the mobility of people and goods across countries and regions [1–3]. These complex infrastructures represent unique technological and economic challenges along their lifecycle [4,5]. A recurrent open topic in the field is the lack of adequate maintenance of this type of infrastructure asset [6,7]. In Canada, 12.4 % of bridges (9661 assets) have been classified to be in poor/very poor condition [8], while 7.5 % of this kind of asset (46 154 bridges) are considered deficient in the USA [9]. In contrast, percentages as up to 39 %, 30 %, and 37 % of deficient bridges are reported in France, Germany, and the United Kingdom, respectively [10]. This issue has motivated researchers to explore the phenomena that negatively impact their structural response [11], and develop more efficient and better monitoring strategies [12] and damage detection methodologies [13–15] that could improve bridge management and operations.

Among the different existing bridge typologies, suspension bridges are especially suitable to cover long spans [16–18]. A suspension bridge is one in which the deck is carried by vertical hangers supported by main cables suspended between tall piers and normally anchored at each end of the bridge to the ground [19]. Examples of iconic suspension bridges around the world are the historic Golden Gate Bridge built in 1937 in San Francisco Bay, USA, with a main span of 1280 m (once the longest single-span bridge in the world) [20] and the 1915 Çanakkale Bridge in Türkiye, with the current longest bridge span in the world (2023 m) opened in 2022 [21]. In suspension bridges, the main cables are of utmost importance because their failure would cause the bridge to collapse as a whole [22]. Main cables are fabricated with hundreds or thousands of individual high-strength steel wires bundled together [23]. Although the bundled wires are typically coated to avoid corrosion, with time and exposure to changing climate and the harsh surrounding environment, the coating layer will degrade and fail [24,25]. This will lead to the inevitable occurrence and acceleration of corrosion in terms

* Corresponding author.
E-mail addresses: alejand@oslomet.no (A. Jimenez Rios), moseg7662@oslomet.no (M.E.A. Ben Seghier), vplevris@qu.edu.qa (V. Plevris), jiandai@oslomet.no (J. Dai).

https://doi.org/10.1016/j.rineng.2024.102723
Received 6 May 2024; Received in revised form 6 August 2024; Accepted 10 August 2024
Available online 13 August 2024

of defects that grow depending on the situation and location of the suspension bridges, which later on can cause failures if no intervention is made [26]. Conversely, the existence of cable coating creates challenging conditions for inspection and monitoring. Current in-depth inspection techniques entail the removal of cable coating and the sampling of wire segments, which are cut and taken to a lab to be analyzed [27,28]. Although novel embedded monitoring systems capable of measuring corrosion rate and environmental conditions have been tested [29,30], their full deployment in existing bridges has not been yet conducted. Corrosion thus has a significant impact on the suspension bridge main cables' remaining strength. Therefore, it is crucial to provide an accurate prediction tool for determining the degree of corrosion in the suspension bridge's main cables.

The complicated chemical, thermodynamic, and electrochemical process known as corrosion causes the metallic wires of the main cables to gradually deteriorate because of exposure to corrosive environments [31–33]. The position of the wires within the bundle and along the cable determines the corrosion degree [34]; wires at the bottom of the cable and those around the perimeter have shown higher corrosion levels [35]. Furthermore, it is yet unclear how climate change may affect the environmental conditions that cause wire corrosion [36]. All these complexities hinder the development of accurate analytical or numerical models capable of accurately estimating corrosion within suspension bridge main cables. Attempts to determine the safety level of main cables in suspension bridges have been undertaken through the implementation of multiscale probabilistic models [37], an inverse reliability method [38], and a partial factor approach based on monitoring data [39]. However, due to the high nonlinearity and complexity of the corrosion process, stochastic approaches can hardly predict corrosion rate variability in an accurate manner [40,41].

Studies related to corrosion in bridges include the work of Karanci and Betti [42] who compiled an extensive database with information from environmental factors affecting the degree of annual corrosion rate in carbon steel. This database was subsequently used to develop and validate a supervised data-based Machine Learning (ML) predictive model [43]. Among the three different algorithms tested, the Support Vector Regression (SVR) model with a Radial Basis Function (RBF) kernel provided the highest performance. It was concluded by Chou et al. [44] that the hybrid Smart Firefly Algorithm-Least Squares Support Vector Regression (SFA-LSSVR) model was capable of improving the prediction accuracy of corrosion due to its dynamic optimization of model hyperparameters. Metaheuristic Optimization Algorithms (MOA) (i.e., Particle Swarm Optimization (PSO), Artificial Bee Colony (ABC), Ant Colony Optimization (ACO), among others) have also been used to solve real-world problems in the fields of electrical and civil engineering [45]. Ben Seghier et al. [46] also used the database compiled by Karanci and Betti to develop and validate a model to predict the annual corrosion rates in suspension bridge main cables. Their framework was based on Multilayer Perceptron (MLP) in combination with different MOA to optimize the calibration of the model hyper-parameters. Ben Seghier et al. [46] experimented with four different variations, all of which yielded higher values of R^2 compared to the SVR algorithm reported by Karanci and Betti [42]. Among these variations, the MLP-MPA algorithm demonstrated the highest performance. An SVR algorithm was also used by Deng et al. [47] to predict fatigue damage in suspension bridges. Their algorithm was trained and tested on a database collected through a novel weight-in-motion (WIM) monitoring system. Therefore, an accurate estimation of the annual corrosion rate is a key element in the development of a time-dependent corrosion rate model.

ML has become a pervasive alternative to solve complex problems, in particular when the physical phenomenology is hard to explain and data can be obtained from underpinning parameters. For instance, Hernández-Díaz et al. [48] implemented a ML strategy to predict the non-linear shear response in reinforced and prestressed concrete beams, thus avoiding convergence problems on conventional Newton-type numerical methods. Yadav et al. [49] reported more precise forecasting values on air pollution levels using ML methods in comparison to model-based numerical approaches. Similarly, Harrou et al. [50] observed higher road traffic flow forecasting performances by implementing ML solutions. Improved performance based ML techniques have been suggested to forecast solar irradiance by Molu et al. [51], to generate surrogate models used on pavements design by Li et al. [52], and to enhance damage detection and classification in bridges by Stagi et al. [53], who validated their novel ML framework on the well-known benchmark case study of the Z24 bridge [54]. Based on this long, but not exhaustive, list of successful ML implementation cases, using sophisticated ML models will produce accurate framework to predict the level of annual corrosion rate in steel cables, which could eventually lead to better safety assessments of existing suspension bridges.

The novelty of our work consists of the development and implementation of a new data-driven framework that employs advanced ML techniques to predict the level of annual corrosion rate in the main cables of suspension bridges, while introducing the Shapley Additive Explanations (SHAP) [55] analysis for the first time to explain the outputs of the proposed ML techniques to solve this problem. The approach implemented here is based on the use of Ensemble Learning (EL) models. The performance of Decision Trees (DT), Random Forest (RF), Adaptive Boosting (ADB), and Extreme Gradient Boosting (XGB) algorithms is

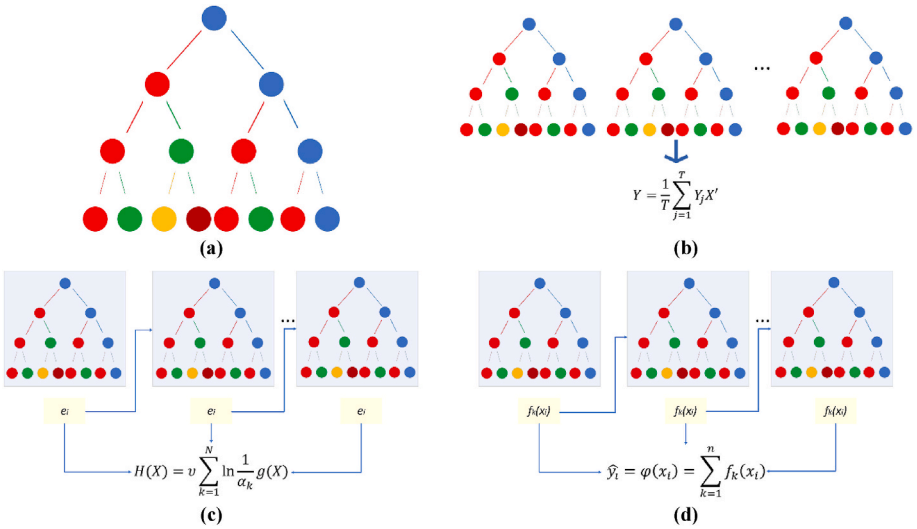

Fig. 1. Schematic representation of the adopted ML predictive models: (a) DT, (b) RF, (c) ADB, and (d) XGB.

assessed. The performance of these models is compared against conventional regression techniques, namely, Multiple Linear Regression (MLR), Ridge Regression (RR), Lasso Regression (LR), and Elastic Net Regression (ENR). Additionally, the impact of the input variables used during the modeling was investigated using the SHAP technique. Our work goes beyond the state of the art and adds value to the existing literature by demonstrating explicit steps on how to employ ML-based explainable models to address the annual corrosion rate in the main cables of suspended bridges. The remainder of the manuscript is organized as follows: Section 2 outlines the adopted methodology, providing detailed descriptions of the characteristics of each implemented algorithm. Section 3 presents the framework implemented for estimating the annual corrosion rate. In Section 4 the obtained results are shown and discussed. Finally, Section 5 offers concluding remarks.

2. Methodology

2.1. Regression-based predictive models

The relationship between two or more variables is commonly studied in engineering through statistical regression methods [56–58]. The simplest of those techniques is the linear regression model, which for a single independent variable can be expressed as:

$$Y = \beta_0 + \beta_1 x + \varepsilon \tag{1}$$

where Y is the dependent variable of interest being estimated, β_0 and β_1 are the function intercept and slope, known as regression coefficients, x is the independent variable or regressor, and finally, ε represents a random error term. In this study, four different advanced statistical regression techniques are used to develop a predictive model for the annual corrosion rate, C_{rate}, in main cables of suspension bridges. The subsequent part provides a brief overview of each of these regression-based predictive models.

2.1.1. Multiple Linear Regression (MLR)

MLR is a statistical technique used to examine the relationship between a dependent variable and two or more independent variables [56]. In general, this model can be expressed as follows:

$$Y = \beta_0 + \beta_1 x_1 + \beta_2 x_2 + \ldots + \beta_k x_k + \varepsilon \tag{2}$$

where k is the considered number of independent variables (i.e. regressors), while β_j, $j = 0, 1, \ldots, k$, are the regression coefficients. The latter are commonly computed using the least squares method, which assumes that the estimator is unbiased. MLR provides relatively good results when there are no significant dependencies within regressors (multicollinearity) [56].

2.1.2. Ridge Regression (RR)

RR is a linear regression technique used to address the problem of multicollinearity and overfitting in MLR. This is achieved by dropping the assumption of an unbiased estimator [59]. The ridge estimator, $\widehat{\boldsymbol{\beta}}_{\boldsymbol{R}}$, can be found by solving the following equation:

$$(\boldsymbol{X}'\boldsymbol{X} + \lambda \boldsymbol{I})\widehat{\boldsymbol{\beta}}_{\boldsymbol{R}} = \boldsymbol{X}'\boldsymbol{y} \tag{3}$$

where $\boldsymbol{y}$ is the vector of dependent variables, $\boldsymbol{X}$ the matrix of independent variables, $\boldsymbol{I}$ the identity matrix, and λ is a strictly positive coefficient [60].

2.1.3. Lasso Regression (LR)

LR is a regression technique used for variable selection and regularization. It assumes the sparsity of the regression coefficients and prevents the MLR overfitting [61]. In LR, regression coefficients are estimated by solving Equation (4):

$$\underset{\beta_0,\beta}{\text{minimize}} \sum_{i=1}^{N} \left(y_i - \beta_0 - \sum_{j=1}^{p} x_{ij}\beta_j \right)^2 \text{ subject to } \|\beta\|_1 \le t \tag{4}$$

where $\|\beta\|_1$ denotes the l_1 norm of β, where t is a user-specified meta parameter. l_1 ensures the problem convexity, which reduces the computational cost.

2.1.4. Elastic Net Regression (ENR)

ENR is an advanced regression technique that combines both LR and RR methods to address the limitations of each approach [61]. To estimate the regression coefficients, the ENR solves the following convex problem:

$$\underset{(\beta_0,\beta)\in R\times R^p}{\text{minimize}} \left\{ \frac{1}{2} \sum_{i=1}^{N} \left(y_i - \beta_0 - x_i^T\beta \right)^2 + \lambda \left[\frac{1}{2}(1-\alpha)\|\beta\|_2^2 + \alpha\|\beta\|_1 \right] \right\} \tag{5}$$

where $\alpha \in [0, 1]$ is a user-specified meta parameter, whereas $\|\beta\|_2$ is the l_2 norm of β.

2.2. ML-based predictive models

Ensemble learning (EL) models are ML techniques that combine the predictions of multiple individual models (i.e. so-called base ML-model or learners; in this case, Decision Trees) to improve the overall predictive performance, generalization, and robustness. The underlying principle of EL models is that, by combining the predictions of multiple base models, the ensemble can frequently yield more accurate and consistent findings than any single model could. Thus, one base model and three EL models are investigated in this work and shown schematically in Fig. 1, whereas briefly discussed in the subsections that follow (further information can be found in Ref. [62]).

2.2.1. Decision Trees (DT)

The DT model, which can be used either for regression or classification purposes, was selected as the base model in this study. This method is a versatile and interpretable hierarchical paradigm that can be visually depicted as a tree structure. While DT is primarily appropriate for classification, it can also be adjusted to address regression problems. The DT concept is to use Equation (6) to generate variance measures within nodes, τ_i, since the dependent variable is continuous in regression problems [63].

$$i(\tau) = \sum (y_i - y_{mean})^2 \tag{6}$$

where y_{mean} denotes the dependent variable mean at the *i-th* node τ_i, while y_i is the *i-th* value of the dependent variable ($i = 1, 2, 3, \ldots n$). The tree is constructed by dividing the "parent" node into "child" nodes based on the independent variable that produces the lowest variance between parent and child.

2.2.2. Random forest (RF)

RF utilizes a randomized feature selection technique to generate a T number of datasets with m samples each (i.e. randomized bootstrap sampling or bagging) [64,65]. Thereafter, individual DT are built from each dataset. Contrary to DT, which splits each node based on optimal criteria, RF uses a subset of randomly generated k features to split the nodes. k is a meta-parameter that influences the process randomness, where values of $k = \log_2 d$ are recommended with d represents the number of independent variables [66]. All T datasets are evaluated, and the outcome is obtained as expressed in the following equation:

$$Y = \frac{1}{T} \sum_{j=1}^{T} Y_j X' \tag{7}$$

where X' represents the unknown instances, Y_j is the j individual deci-

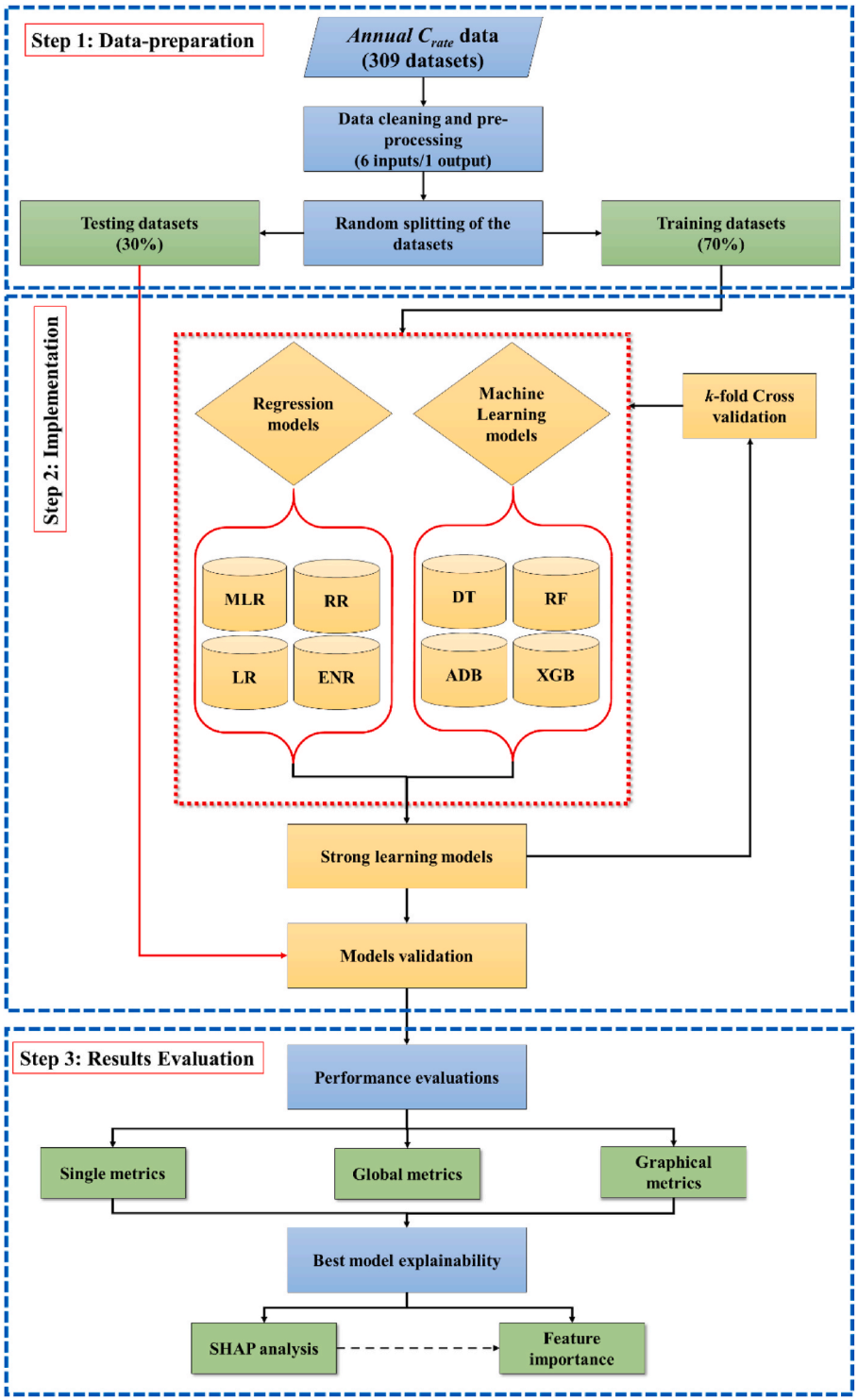

Fig. 2. Proposed framework for modeling the annual corrosion rate in main cables of suspension bridges.

sion tree, and Y denotes the target output.

2.2.3. Adaptive boosting (ADB)

ADB is designed to generate a strong EL model by combining weak learners ($G(\boldsymbol{X})$), thus improving their performance. Each sample can be predicted with $G(\boldsymbol{X})$, which will result in a relative error e_i, as described by Equation (8) [67].

$$e_i = L(y_i, G(X_i)) \tag{8}$$

where $(X_i, y_i)(i = 1, 2, \ldots, m)$ represent the i-th sample, m denotes the total number of samples, and L is the loss function. As expected, these weak learners, $G_k(\boldsymbol{X})$ $k = 1,2,\ldots,N$, will have a poor performance stand-alone. The overall performance will be highly enhanced based on ADB using the expression:

$$H(X) = \upsilon \sum_{k=1}^{N} \ln \frac{1}{\alpha_k} g(X) \tag{9}$$

where $\upsilon \in (0, 1]$ is the learning rate, α_k denotes the weight related to each

Table 1
Descriptive statistical report for the utilized database in this study.

Type	Variables, units	Mean	STD	Min	25^{th} percentile	50^{th} percentile	75^{th} percentile	Max
Inputs	*T*, °C	15.29	8.74	−3.10	10.91	15.7	23.03	29.82
	RH, %	46.05	18.03	0.00	35.00	47.0	58.00	98.00
	TOW, %	68.69	14.10	33.30	63.80	69.2	77.00	91.10
	P, *mm*	882.42	486.83	13.00	513.00	792.0	1208.00	3677.00
	pH, -	4.98	0.86	3.44	4.45	4.9	5.26	7.37
	CL^-, mg/L	12.35	27.17	0.01	0.80	2.4	8.00	192.73
Output	C_{rate}, μm/year	38.52	43.76	3.30	17.90	28.1	41.10	376.70

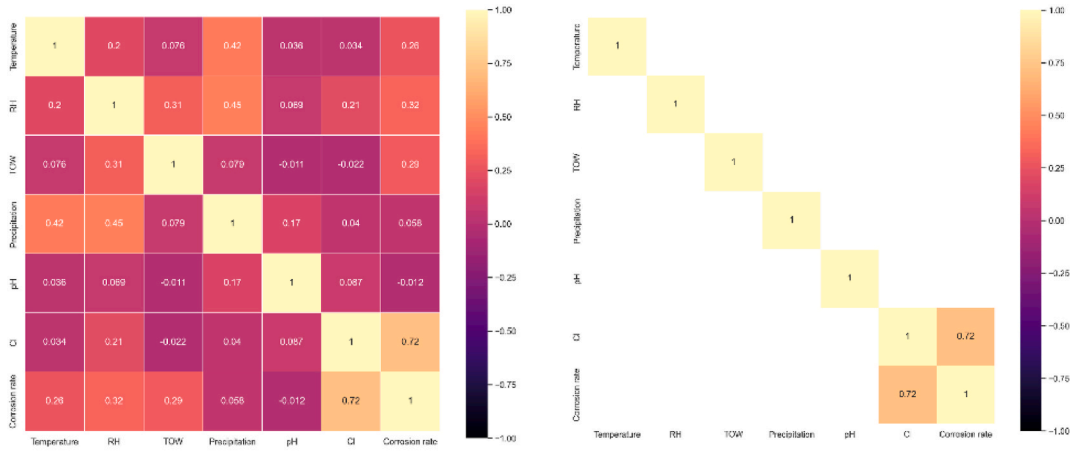

(a) **(b)**

Fig. 3. Pearson correlation matrix between the database variables. (a) All correlations; (b) Only correlations with an absolute value higher than 0.5.

$G_k(\boldsymbol{X})$, while $g(\boldsymbol{X})$ represents the mean of all $\alpha_k G_k(\boldsymbol{X})$ $k = 1, 2, \ldots, N$ products. This iterative process adjust the sample distribution weights using the predicting error, $E = max|Y_i - G(X_i)|$, of the previous iterations.

2.2.4. Extreme gradient boosting (XGB)

XGB is an enhanced version of the Gradient Boosting Regression Tree (GBRT) algorithm [68]. It employs DT as a base learner and builds multiple weak learners in an iterative process. Gradient descent is used to train these weak learners. The optimal solution, accuracy, and complexity of this method are achieved through the implementation of Taylor series to expand the loss function, which contains a regularization term [69]. XGB can be mathematically represented through Equation (10):

$$\widehat{y}_i = \varphi(x_i) = \sum_{k=1}^{n} f_k(x_i), f_k \ni F \tag{10}$$

where F is composed by the DT within the function space, f_k denotes a series of independent functions, x_i and $\varphi(x_i)$ are the i_{th} sample and the function related to the x_i sample, respectively, whereas $\widehat{y}_i$ denotes the model predicted value.

2.3. Shapley Additive Explanations

Shapley Additive Explanations (SHAP) offers both local and global explanations of results thereby enhancing the interpretability of predictive models [70]. It assigns an importance value to each one of the model features when predicting the output which is more consistent with human intuition. This characteristic allows for a better understanding of the model and of how it could be further improved. Eventually, this results in higher levels of user trust [55]. The importance that every model feature may have in the predicted outcome value could be either negative or positive. The former contributes to increasing the magnitude of the response, whereas the latter decreases it. To compute SHAP values, all feature subsets ($S \subseteq F$, where F is the set of all features) are retrained in the model. The importance value of each feature in the model is obtained by comparing a trained model with such feature included, $f_{SU\{i\}}$, against another without it, f_S. The comparison is performed on the current input as presented in Equation (11):

$$f_{SU\{i\}}\left(x_{SU\{i\}}\right) - f_S(x_S) \tag{11}$$

where x_S represents the input feature values in the S set. Finally, Shapely regression values are computed as a weighted average of all differences in the possible subsets, $S \subseteq F \backslash \{i\}$, following Equation (12) [55]:

$$\phi_i = \sum_{S \subseteq F \backslash \{i\}} \frac{|S|!(|F| - |S| - 1)!}{|F|!} \left[f_{SU\{i\}}\left(x_{SU\{i\}}\right) - f_S(x_S) \right] \tag{12}$$

3. Implementation

3.1. Proposed framework

The annual corrosion rate, C_{rate} ($\mu m/year$) in suspension cable bridges is predicted using the framework depicted in Fig. 2. The aim is to assess and evaluate the comparative efficiency of ML and regression models in predicting the corrosion behavior, and to identify the best approach for examining the influence of input variables on the outcome. To accomplish this, variables affecting the annual corrosion rate, C_{rate}, were identified, and the relevant data were gathered and preprocessed (Section 3.2). These datasets were utilized in training and testing the predictive models. The modeling process is carried out using four ML models (DT, RF, ADB, and XGB), of which three are EL models, and four regression models (MLR, RR, LR, and ENR). To determine the performance of each model and its effectiveness, the analysis employed various comparative evaluation criteria (Section 3.3). Finally, the SHAP approach is employed to explain the best predictive model and to

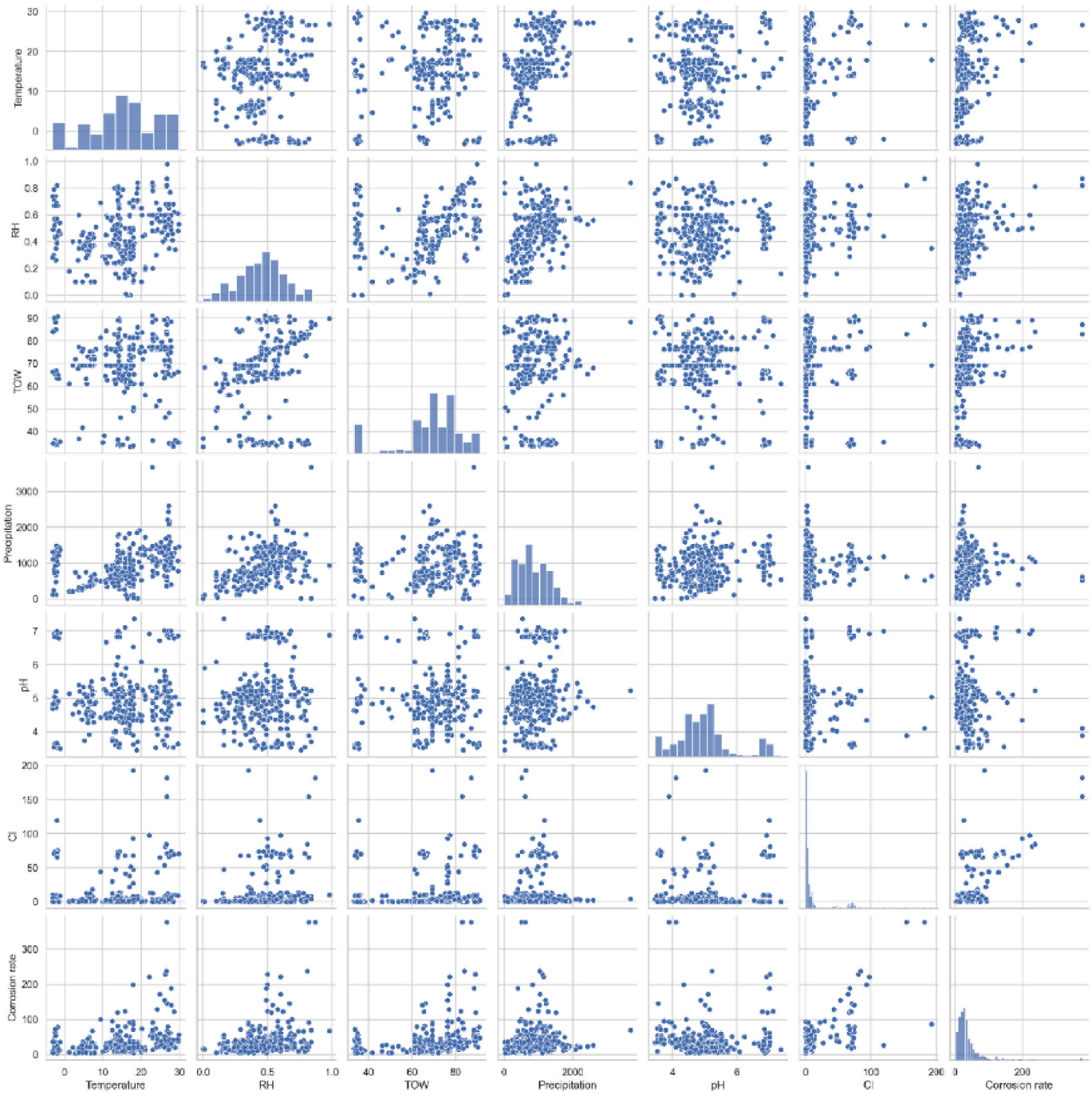

Fig. 4. Pair plot for data distribution between the input-output variables.

analyze the most influential variables and their impact on the output trend. It is worth noting that all the coding is done using the Python platform and its available libraries.

The data cleaning and pre-processing procedure include in general, first, data understanding (numerical data, identifying the inputs and outputs), identifying and handling potential missing values (no missing values were identified), dealing with duplicated data, if discovered (no duplicated data was discovered), and handling outliers using box plots (all data were used in the study), statistical analysis (Section 3.2), data normalization to a similar range to prevent features with larger scales from dominating the model, and finally data splitting before beginning the modeling process.

Normalizing the input and output variables during the modeling process is crucial to enhance the model's effectiveness. This ensures that all variables are on the same scale, preventing biased or overly scrutinized results. The purpose of normalization is to transform the numerical values in a dataset to a standard scale while preserving meaningful variations between value ranges. Every variable in this dataset has been normalized to fall between −1 and 1, using the following formula:

$$x_{Normalized} = \frac{2(x_{Actual} - x_{min})}{(x_{max} - x_{min})} - 1 \tag{13}$$

where x_{Actual} denotes the actual annual corrosion rate dataset, x_{min} and x_{max} denotes the dataset's minimum and maximum values, respectively. After the normalization process, the datasets are randomly split into two subsets: the training dataset, which constitutes 70 % of the total dataset, and the testing dataset, which comprises the remaining 30 %. It is worth

Table 2
Performance metrics utilized to evaluate the behavior of the studied models.

Metric: statistical significance	Equation	Equation #
Root Mean Square Error (RMSE): represent the stander error and used to compare the absolute deviation of various models.	$RMSE = \frac{1}{n}\sum_{i=1}^{n}\left(C_{rate,i}^{Act} - C_{rate,i}^{Pre}\right)^2$	(14)
Mean Absolute Error (MAE): represents a statistical measure used to estimate the average value of the absolute deviation, where the sum of predicted and observed individual of the database are used.	$MAE = \frac{1}{n}\sum_{i=1}^{n}\left\|C_{rate,i}^{Act} - C_{rate,i}^{Pre}\right\|$	(15)
Coefficient of determination (R^2): used to determine the correlation for a fraction of the estimated and predicted values.	$R^2 = 1 - \frac{\sum_{i=1}^{n}\left(C_{rate,i}^{Act} - C_{rate,i}^{Pre}\right)^2}{\sum_{i=1}^{n}\left(C_{rate}^{Avg} - C_{rate,i}^{Pre}\right)^2}$	(16)
Confidence Interval (CI): is introduced to calculate and compare the performance of several models and calculated using the product of two metrics	$CI = WI \times NSE$	(17)
Willmott's Index of agreement (WI): used as a cross-comparison between models based on the standard error values.	$WI = 1 - \frac{\sum_{i=1}^{n}\left(C_{rate,i}^{Act} - C_{rate,i}^{Pre}\right)^2}{\sum_{i=1}^{n}\left(\left\|C_{rate,i}^{Pre} - C_{rate}^{Avg}\right\| + \left\|C_{rate,i}^{Act} - C_{rate}^{Avg}\right\|\right)^2}$	(18)
Nash–Sutcliffe Efficiency (NSE): indicates the model efficiency, whereas a goodness-of-fit measure is calculated based on the error variance and observed variance.	$NSE = 1 - \frac{\sum_{i=1}^{n}\left(C_{rate,i}^{Act} - C_{rate,i}^{Pre}\right)^2}{\sum_{i=1}^{n}\left(C_{rate,i}^{Act} - C_{rate}^{Avg}\right)^2}$	(19)
Uncertainty at 95 % (U95): indicates the 95 % confidence interval (1.96 standard errors).	$U95 = 1.96 \times \sqrt{Standard\ deviation^2 - RMSE^2}$	(20)

$C_{rate,i}^{Act}$: Actual value of the i_{th} annual corrosion rate from the test result measurements.
$C_{rate,i}^{Avg}$: Average value of the *i_th* annual corrosion rate from the test result measurements.
$C_{rate,i}^{Pre}$: Predicted value of the *i_th* annual corrosion rate from the test result measurements.

noting that *K-fold* cross-validation is used on the training data to minimize overfitting issues during the model development phase.

3.2. Data description and preprocessing

A thorough database is required to gain a better understanding of the complex relationship between environmental conditions and the annual corrosion rate, C_{rate}, in the main cables of suspension bridges. To do this, a database that Karanci and Betti [42,43] compiled and arranged from numerous atmospheric corrosion tests on carbon steel conducted across several countries is examined and used. The database comprises 309 datasets, gathered from more than 250 distinct test locations spread over 33 countries. The extensive collected data sheds light on how different variables impacted the corrosion rate, C_{rate} of carbon steel specimens over time (years). Six environmental factors are classified as independent variables, while the final factor—the annual corrosion rate, C_{rate}—is classified as a dependent variable and expressed in $\mu m/year$. The independent variables, also defined as the input parameters during the modeling process include: (i) Temperature (T, °C), (ii) Relative humidity (RH, %), (iii) Duration of moisture on the metal's surface (TOW, %), (iv) Annual precipitation (P, mm), (v) Rainwater pH (pH), and (vi) Chloride ion concentration (CL^-, mg/L). These variables collectively represent the atmospheric conditions with a significant influence on the value of the dependent variable, also referred to as the output parameter in this study.

Table 1 reports the statistical summary of each variable within the database. The statistics of interest for every independent and dependent variable include the mean (X_{Mean}), standard deviation (X_{STD}), minimum value (X_{Min}), maximum value (X_{Max}), as well as the 25th, 50th, and 75th percentiles. From this table, it can be observed that the different variables spread over ranges with diverse orders of magnitude. For example, RH can go from 0 to 0.98 (all values are contained within a single unit), whereas CL^- can go from 0.1 up to 192, covering three orders of magnitude. Therefore, as previously mentioned, a normalization process was implemented.

Fig. 2 displays a Pearson correlation matrix that helps visualize the correlation between the database variables. All ranges (−1 to 1) are shown in Fig. 3 (a) whereas Fig. 3 (b) includes only correlation coefficients with an absolute value higher than 0.5. It is worth noting that a strong positive correlation is observed between chloride ion concentration (CL^-) and the dependent variable of interest (C_{rate}), as the corresponding Pearson correlation coefficient has a value of 0.72. A moderate to low correlation is observed between the rest of the independent variables and the annual corrosion rate, C_{rate}, all being positive apart from pH.

Fig. 4 illustrates the pair plots as a series of scatterplots and histograms of the variables compiled within the described database. From the diagonal of this figure, only RH presents a clear normal distribution. TOW distribution appears to be left-skewed, whereas that pH and the precipitation are right-skewed. Moreover, T has sort of a uniform distribution and CL^- an exponential distribution. Furthermore, there is a lack of clear correlation between any of the environmental variables and the annual corrosion rate, C_{rate}. This is evidence of the complexity and high nonlinearity characteristic of the corrosion phenomena, which justifies the utilization of advanced ML algorithms to improve predictability performance.

3.3. Evaluation metrics

To have a better understanding of the performance evaluation of the different proposed regression and ML predictive models, a series of statistical and graphical evaluation metrics were adopted [71,72]. The graphical comparative illustration consists of the Taylor diagram (as a global graphical indicator) and scatterplots (as a single graphical indicator), while the comparative statistical indicators are included in Table 2. Note that a single statistical indicator (e.g., RMSE, MAE, and R^2) only uses a relationship between the anticipated and measured values of C_{rate}, whereas a global indicator employs several single indicators (e.g., CI, U95, and Taylor diagram [73]). For a given model, higher values of R^2, WI, NSE, and CI indicate higher agreement between the predicted and measured values, whereas lower values of RMSE, MAE, and U95 indicate a lower predicted error. Both RMSE and MAE values can range from 0 to ∞, with 0 indicating a perfect fit to the data. R^2 and WI vary between 0 and 1, being 1 a perfect agreement while 0 a sign that the model explains none of the variability observed in the response. NSE could range between −∞ and 1, where an efficiency of 1 corresponds to perfect predictive performance, while an efficiency of 0 indicates that the model predictions are as accurate as the mean of the observed data, whereas a negative value occurs when the residual variance is larger than the data variance.

Table 3
Performance evaluation of the regression-based predictive models.

Phase	Models	RMSE	MAE	NSE	WI	CI	U95
Training	MLR	22.9910	16.3312	0.7583	0.6993	0.5303	46.1343
	RR	23.5276	15.7075	0.7469	0.6413	0.4790	47.1070
	LR	21.9105	15.2360	0.7805	0.6613	0.5162	43.8989
	ENR	**19.8590**	**14.3278**	**0.8197**	**0.7029**	**0.5761**	**39.6731**
Testing	MLR	29.4214	16.3912	0.3100	**0.7694**	0.2385	58.2252
	RR	20.4419	14.4800	0.6669	0.6850	0.4568	40.5453
	LR	18.8339	13.4275	0.7173	0.6701	0.4806	37.7432
	ENR	**18.2453**	**13.3103**	**0.7347**	0.6819	**0.5010**	**36.5653**
Overall	MLR	24.9201	16.3492	0.6239	**0.7203**	0.4428	49.7616
	RR	22.6019	15.3392	0.7229	0.6544	0.4724	45.1385
	LR	20.9875	14.6935	0.7615	0.6639	0.5055	42.0522
	ENR	**19.3749**	**14.0226**	**0.7942**	0.6966	**0.5536**	**38.7408**

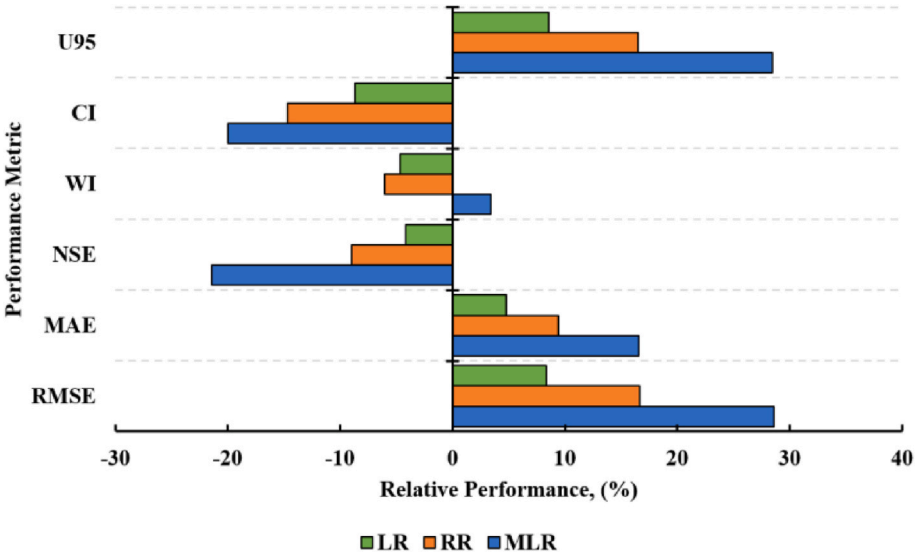

Fig. 5. Relative metrics performance comparison for the regression-based predictive models.

Table 4
Performance evaluation of the ML-based predictive models.

Phase	Models	RMSE	MAE	NSE	WI	CI	U95
Training	DT*	0.0000	0.0000	1.0000	0.7500	0.7500	0.0000
	RF	9.5787	5.2450	0.9581	0.7138	0.6839	19.7700
	XGB	**1.6045**	**1.1450**	**0.9988**	**0.7466**	**0.7457**	**4.0103**
	ADB	11.0305	8.4924	0.9444	0.7349	0.6940	20.8970
Testing	DT	37.9995	16.9968	−0.1509	**0.7774**	−0.1173	74.9782
	RF	14.8763	10.9661	0.8236	0.6666	0.5490	29.7841
	XGB	**8.8579**	**6.7326**	**0.9375**	0.7233	**0.6780**	**18.3155**
	ADB	14.5620	12.1730	0.8310	0.7009	0.5824	25.9365
Overall	DT	11.3998	5.0990	0.6547	**0.7582**	0.4898	22.4935
	RF	11.1680	6.9613	0.9177	0.6997	0.6434	22.7743
	XGB	**3.7805**	**2.8213**	**0.9804**	0.7396	**0.7254**	**8.3019**
	ADB	12.0899	9.5966	0.9104	0.7247	0.6605	22.4088

*DT model showed over-fitting.

4. Results and discussion

This section presents and discusses the modeling results based on the performance evaluation of each predictive model. Additionally, the discussion is expanded using SHAP results, which are graphically presented as force plots, global feature importance bar plots, and beeswarm summary plots.

4.1. Performance evaluation using statistical metrics

4.1.1. Regression based predictive models

The statistical performance evaluation of the regression-based predictive models implemented in this study is presented in Table 3. This includes the outcomes attained in the testing, training, and overall phases—the latter of which consists of 30 % testing and 70 % training. Additionally, two global metrics—CI and U95—as well as four single statistical metrics—RMSE, MAE, NSE, and WI—are employed. The results show that the ENR model performs better for the training data across all calculated statistical metrics (i.e. higher values of CI, NSE, and WI, and lower values of RMSE, MAE, and U95). For the testing data, the best-performing regression model in terms of RMSE, MAE, U95, and CI was also the ENR. However, the MLR resulted in a higher WI value. Similarly, the overall results show a better performance by the ENR model for all statistical metrics apart from WI, where the MLR model

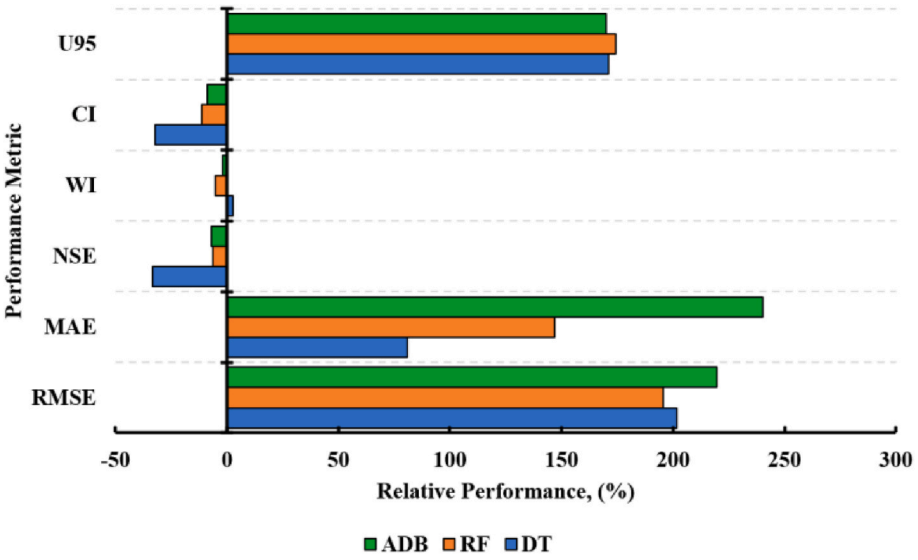

Fig. 6. Relative metrics performance comparison for the ML-based predictive models.

provided the highest value. In general terms, the regression-based predictive models implemented in this paper show low adaptation to the complexity of the database, indicating a relatively low performance to predict C_{rate} values.

The overall performance of the different models is subjected to a relative comparison. The reference model is the ENR, which has been identified as the best-performing regression model. The comparison is performed through a relative percentage comparison, computed as shown in Equation (21). Fig. 5 shows the relative metric performances of the different regression-based predictive models in comparison to ENR. Apart from the *WI* value obtained with the MLR model, (WI_{MLR} was 3.4 % higher than WI_{ENR}) the ENR performed better than any other regression model. The $RMSE_{ENR}$ shows an improvement of 28.62 %, 16.66 %, and 8.32 % compared to the $RMSE_{MLR}$, $RMSE_{RR}$ and $RMSE_{LR}$

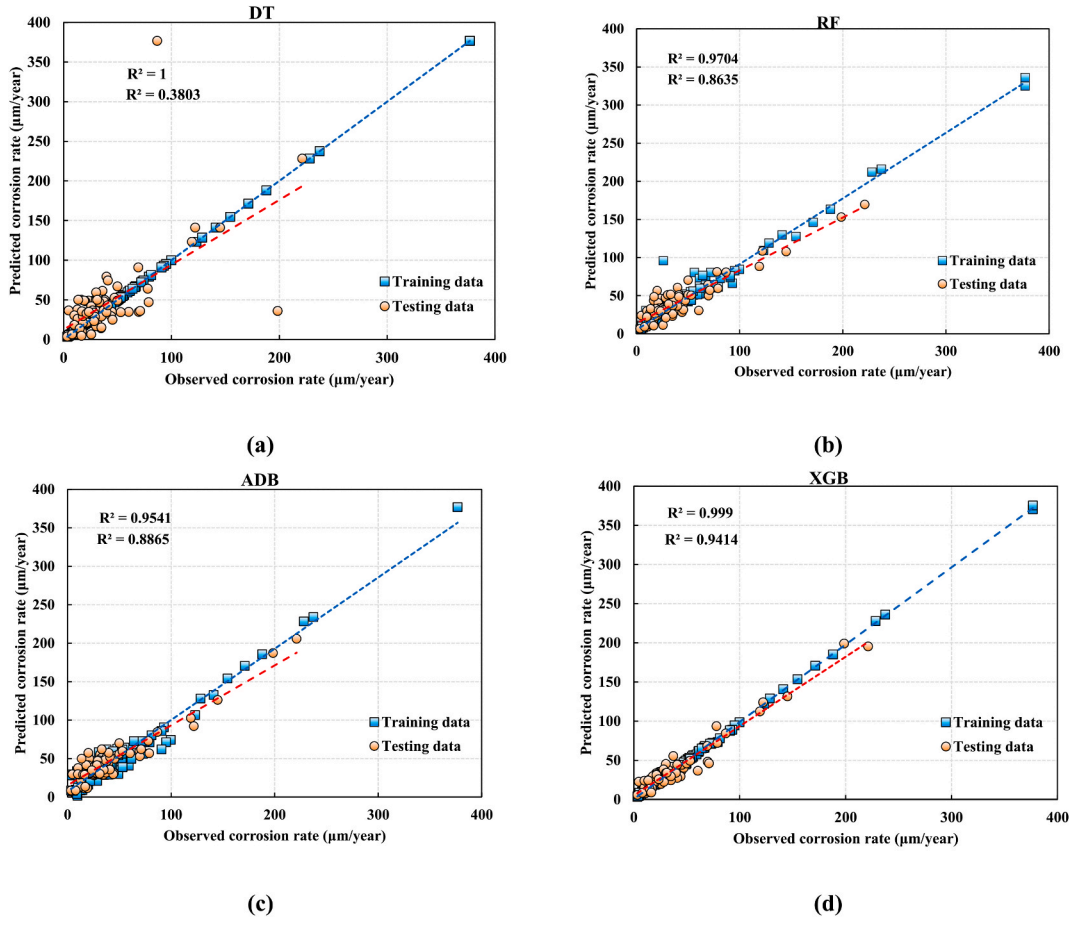

Fig. 7. Scatter plots for the regression models: (a) MLR, (b) RR, (c) LR, and (d) ENR.

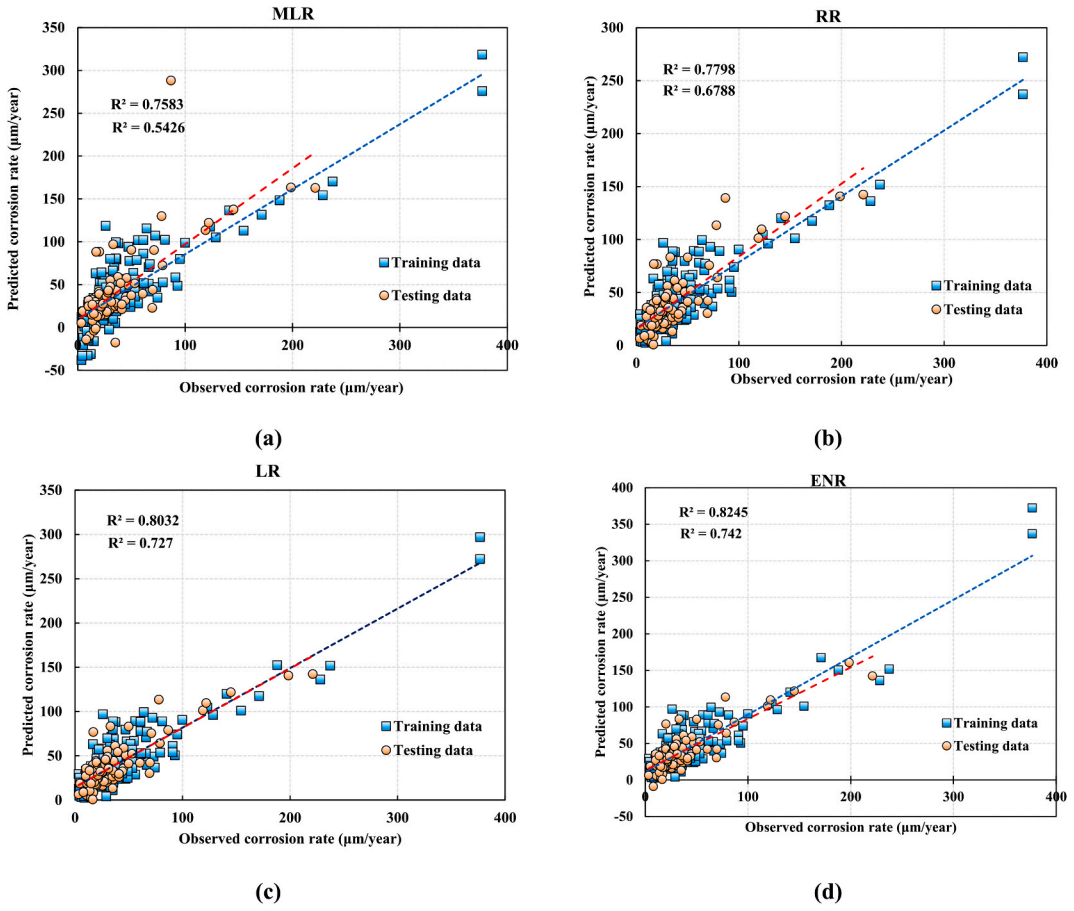

Fig. 8. Scatter plots for the ML models: (a) DT, (b) RF, (c) ADB, and (d) XGB.

values, respectively.

$$Relative\ comparison = \frac{(Comparison_{i\ metric} - Reference_{i\ metric})}{Reference_{i\ metric}} * 100 \qquad (21)$$

4.1.2. ML-based predictive models

The performance evaluation metrics for the ML-based predictive models are presented in Table 4. According to the statistical metrics, the DT model exhibited overfitting during the training phase, as evidenced by a perfect fit between the predicted and measured data, which significantly dropped during the testing phase. On the other hand, the best-performing ensemble learning algorithm during both phases is the XGB, as it provided the lowest values of RMSE, MAE, and U95 along with the highest values of CI and NSE. XGB was surpassed by DT in terms of WI. Similar comments can be made for the overall performance scenario of the ML-based predictive models, as can be seen in the overall rows of Table 4. According to the observed performance metric values, the DT model yielded the lowest performance among the ML models, thus indicating poor adaptability to solve the presented problem.

In general, the performance of the ML-based predictive models is superior to that of the regression-based models. This claim is supported by the comparatively lower RMSE, MAE, and U95 values provided by the ML-based predictive models. On the other hand, in terms of WI, NSE, and CI, the regression-based models were the ones with higher metric values. The XGB was not only the best-performing ML predictive model but the best-performing one among the entire variety of implemented and assessed models. These results highlight the suitability of EL models to be implemented in C_{rate} prediction.

Fig. 6 shows the relative metric performances of the different ML-based predictive models in comparison to XGB, which has been identified as the overall best-performing model. The XGB model performed better than any other model in all different performance metrics, apart from the *WI* value obtained with the DT model, (WI_{DT} was 2.51 % higher than WI_{XGB}). The $RMSE_{DT}$, $RMSE_{RF}$ and $RMSE_{ADB}$ were 202 %, 195 %, and 220 % higher than the $RMSE_{XGB}$ value respectively. The XGB results outperformed the best ML-model in the literature, proposed by Ben Seghier et al. [46], in terms of RMSE and MSE by 3.5 times (RMSEBen Seghier = 13.1837 µm/year) and 3.3 times (MAEBen Seghier = 9.3932 µm/year), respectively.

4.2. Performance evaluation using graphical metrics

The performance of the different predictive models is visually assessed using scatter plots and Taylor diagram plots [73], in which the first presents the degree of agreement, while the second illustrates the degree of correspondence between the predicted and measured. Such diagrams present in a single plot three statistics, namely, correlation coefficient (R), *RMSE*, and standard deviation (σ), which allow for a straightforward visual comparison of the predictive model's performance (the closer a model's marker is to the reference point, the higher the model's performance is).

4.2.1. Regression-based predictive models

Fig. 7 presents the scatter plots, including regression lines, and corresponding R^2 values of the different employed regression models, both for the training and testing sets. From these plots, it can be observed that the ENR has the highest performance, where it resulted in the highest R^2 values during the training (0.824) and testing (0.742) phases. The high performance of the ENR model could be explained by the fact that this regression technique combines both advantages of LR and RR methods, thus addressing the limitations of each approach. The performance of

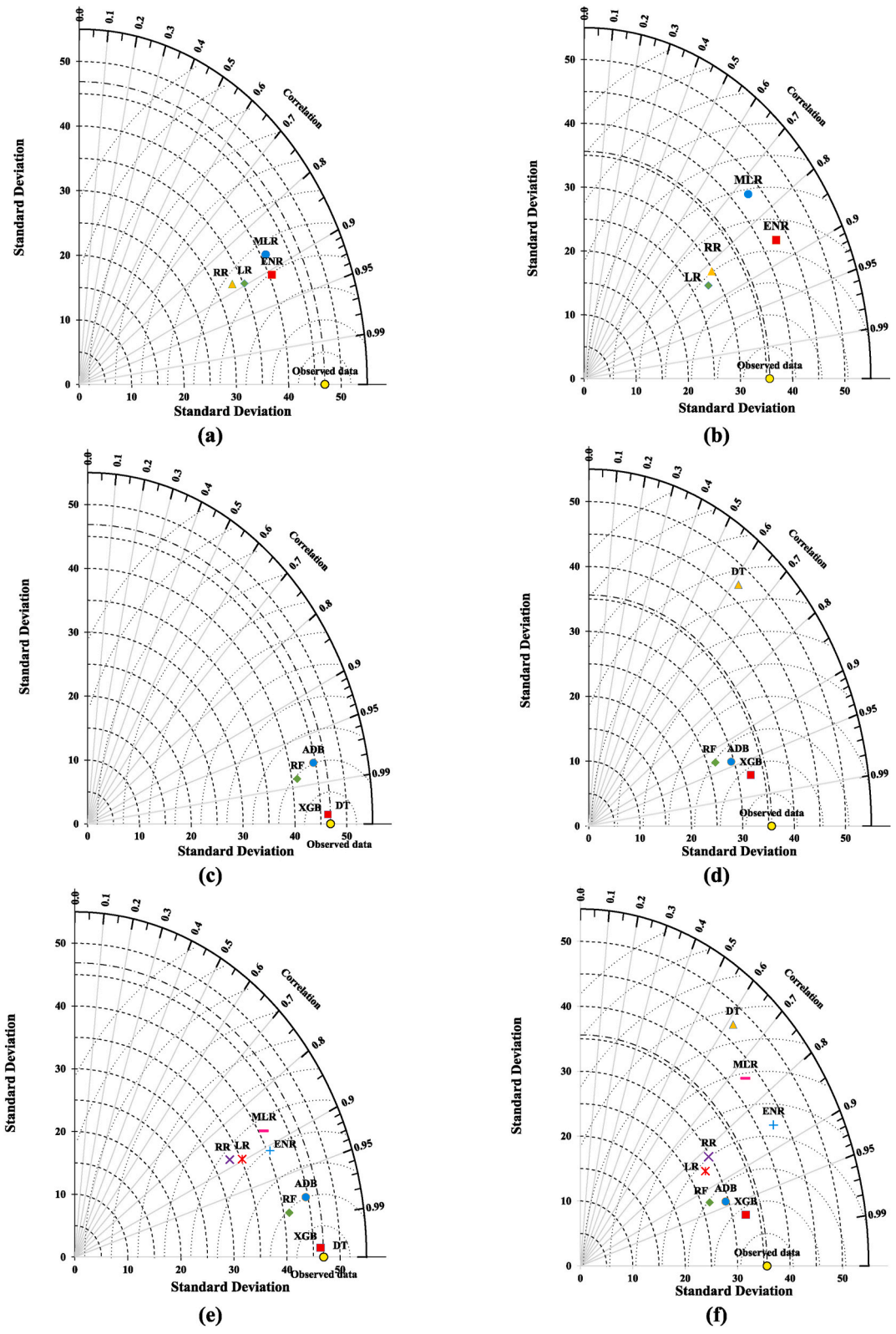

Fig. 9. Taylor diagram plots for: Regression-based predictive models: (a) training and (b) testing, ML-based predictive models (c) training and (d) testing, All predictive models during (e) training and (f) testing phases.

the regression-based predictive models could be ranked as ENR > LR > RR > MLR in terms of R^2. Apart from the relatively poor predictive results of the other regression models, another significant limitation to note is that these models produced negative values for the annual corrosion rate (this is particularly visible for MLR). This is illustrated by the dots plotted below the horizontal axis, near the origin, which bear no physical significance. Therefore, the use of these models could lead to misleading values for the annual corrosion rate, C_{rate}.

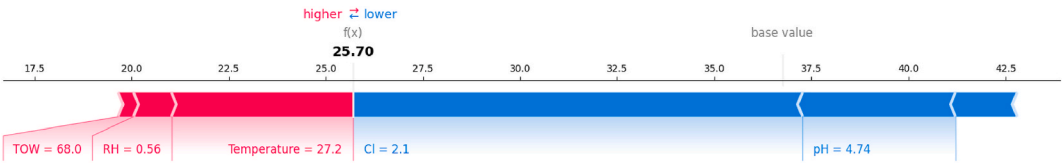

Fig. 10. SHAP force plot based on the XGB model.

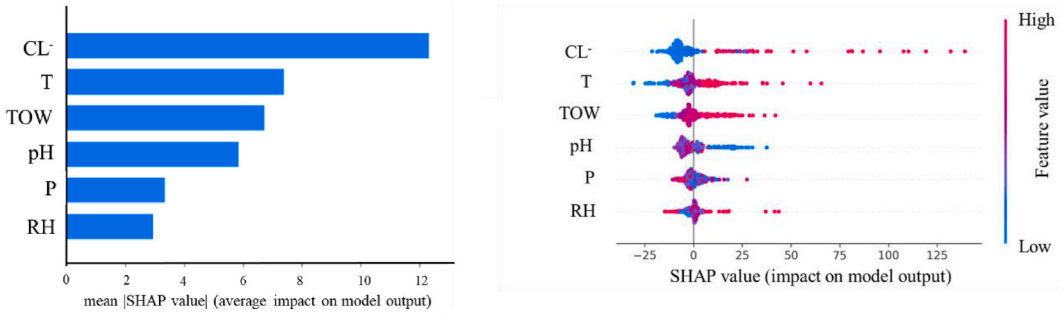

Fig. 11. SHAP plots for the XGB model: (a) Global feature importance bar plot, and (b) Beeswarm summary plot.

4.2.2. ML-based predictive models

Similarly, the scatter plots for the ML-based predictive model are plotted in Fig. 8. Overall, the R^2 values of all these models is higher than those of the regression-based predictive models. It can be observed that DT achieved perfect agreement during the training phase with $R^2 = 1$ indicating overfitting as the R^2 value during the testing phase is 0.38, which is the lowest among all models. The EL model with the highest performance is XGB, which provided R^2 values of 0.999 and 0.941 for the training and testing phases, respectively. As a result, the performance of the ML models can be ranked as follows: XGB > ADB > RF > DT. In addition to their already discussed superior performance, it's notable that EL models never produce negative values for the annual corrosion rate, C_{rate} under any conditions, thereby maintaining the physical significance of the required predictive task. The XGB outperformed the ADB, RD, and DT models in terms of R^2 prediction, by 4.88 %, 4.42 %, and 17.07 %, respectively. Furthermore, the results are improved by 2.9 % compared to the best ML-model in the literature, proposed by Ben Seghier et al. [46].

4.2.3. Global evaluation

A more holistic way of visually comparing the model's performance evaluation is through Taylor diagram plots. Fig. 9 (a) and (b) present the Taylor diagrams of the regression-based predictive models. It can be observed that for both the training and the testing phases, the ENR model is the nearest to the observed data location. Fig. 9 (c) and (d) show the Taylor diagrams of the ML-based predictive models. It can be claimed that although both DT and XGB practically overlap close to the observed data point for the training phase, the XGB model outperforms all other ML models during the testing phase. Finally, both regression and ML predictive models' performance can be observed in Fig. 9(e) and (f), which confirms the outperformance of the XGB model compared to all other investigated models in this study.

4.3. SHAP-based results

A SHAP analysis was conducted to improve the model interpretability and boost the level of trust in the reported results. This investigation focused on the XGB model, which was determined to be the best-performing model among the examined approaches. The SHAP force plots for the XGB model are presented in Fig. 10, which provide a visual representation of the SHAP values using an additive force layout. In these plots, red regions indicate parameters that increase the prediction towards the model output when included, while blue regions signify a decrease towards the output prediction when incorporated. This plot is effective at illustrating how the model reached its decision. In Fig. 10 it can be observed that *TOW*, *RH* and *T* contribute to increasing the predictive output values of the XGB model, while CL^-, *pH*, and *P* reduced the prediction values. Moreover, it can be argued that the feature with the greatest contribution is CL^-, followed by *T* and *pH*. This statement is supported by the length of the bar assigned to each of the features represented in the horizontal scale. The final accumulated output value, based on the feature values shown in the figure, resulted in an annual corrosion rate, Crate = 25.70 μm/year.

In Fig. 11 (a) the global importance of each feature is determined by calculating the mean absolute value across all provided samples. CL^- emerges as the most influential parameter, aligning with the findings of Pearson correlation analysis. The parameters that follow in importance after CL^- are *T* and *TOW*. In Fig. 11 (b), an information-rich summary illustrates how the top features in the dataset influence the model's output. Each instance of the provided explanation is depicted by a single dot on each feature row. The horizontal position of the dot is determined by the SHAP value of that feature, with dots accumulating along each feature row to demonstrate density. Color is used to display the original value of a feature. For instance, points with negative SHAP values of CL^- suggest a lower likelihood of corrosion occurrence. By default, the features are ordered using the mean absolute SHAP value for each feature. However, this order prioritizes broad average impact over rare but high-magnitude impacts. To identify features with significant impacts for individual instances, sorting by the max absolute value is recommended. As can be observed, increasing the selected values results in a significant acceleration of the corrosion process, with CL^- having the biggest influence (red dots on the right side), followed by *T* and *TOW*. An intriguing point is that an increase in pH would result in decreased corrosion acceleration, which is consistent with experimental investigations, where corrosion tends to be higher in an acidic environment rather than in an alkaline environment [74].

Fig. 12 represents the dependence scatter plots, which demonstrate the effect of a single feature on the model's predictions as a function of other feature values, also known as interaction effects, with each dot representing a single prediction (row) from the dataset. The x-axis indicates the value of the feature, whereas the left y-axis represents its SHAP, indicating how much knowing that feature's value influences the

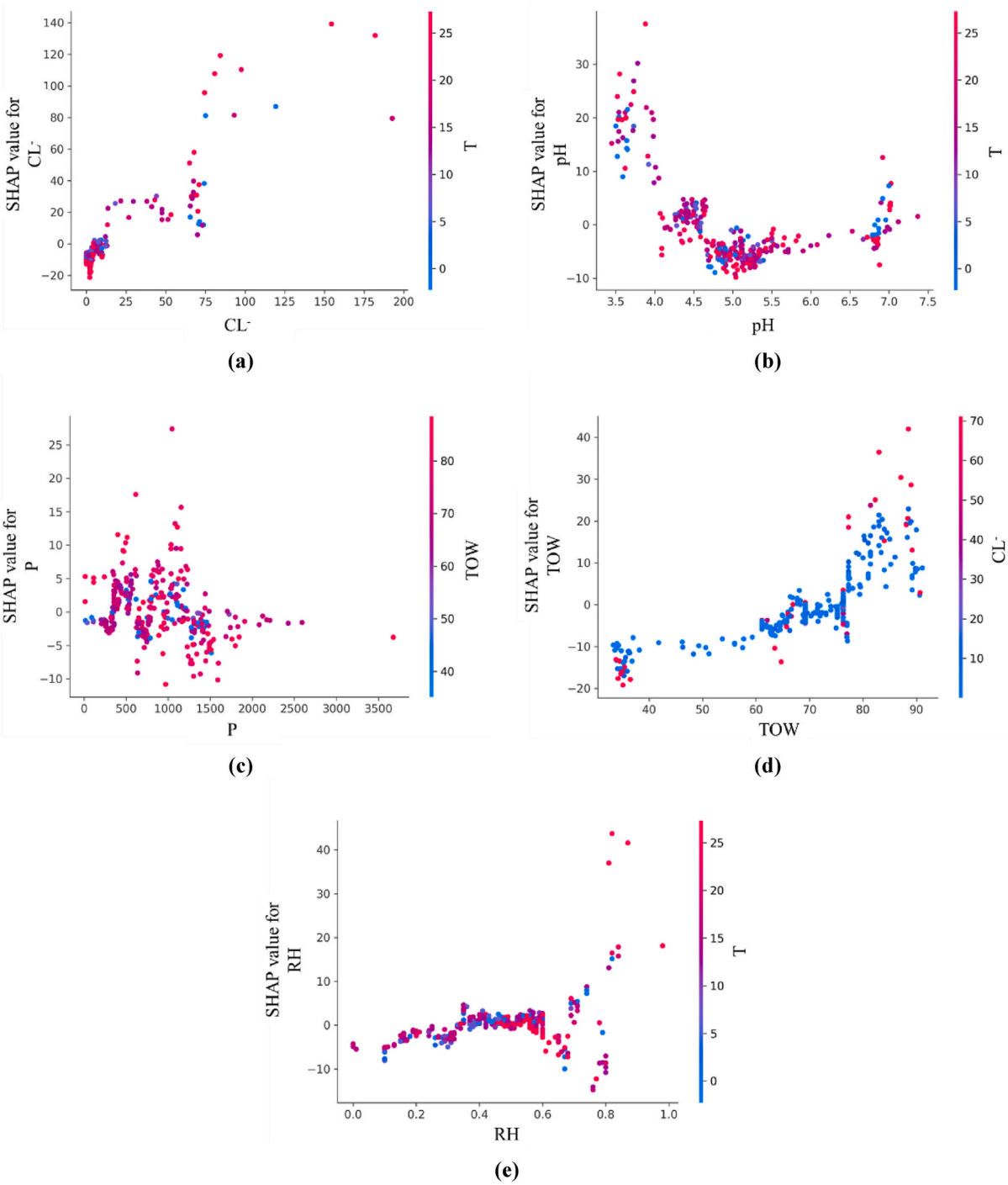

Fig. 12. Dependence scatter plots with interaction effects for the XGB model: (a) CL^- and T, (b) pH and T, (c) P and TOW, (d) TOW and CL^-, and (e) RH and T.

model's output for that sample's prediction. To illustrate the interaction effects, dots are colored based on a second feature value (right y-axis). As it is not possible to identify a distinct vertical pattern of coloring in any of the subfigures, it can be stated that based on the SHAP interaction effects of the analyzed features, there is no significant interaction impact between the used variables. This observation does not imply a negative outcome or render the SHAP analysis ineffective; rather, it indicates the absence of evident interaction based on the SHAP values. Nonetheless, the effect of individual parameters remains visible in Fig. 11, as previously discussed.

5. Conclusions

Predicting the annual corrosion rate in suspension bridge main cables presents a multidimensional challenge characterized by intricate, nonlinear dynamics with chaotic patterns and stochastic behavior. In this study, we evaluated the efficiency of various ML models—namely, decision tree (DT), random forest (RF), adaptive boosting (ADB), and extreme gradient boosting (XGB), in predicting the annual corrosion rates. In addition, the performance of these models was benchmarked against four traditional regression methods, namely, Multiple Linear Regression (MLR), Ridge Regression (RR), Lasso Regression (LR), and Elastic Net Regression (ENR). The analysis leveraged a comprehensive

database comprising 309 measurements of annual corrosion rates of carbon steel specimens, recorded across diverse atmospheric conditions, and tested in 33 different countries over the course of a year. The performance of these models was then evaluated using various metrics, with the best model explained using the SHAP approach. The key findings derived from the acquired results are summarized as follows.

- Regression-based models exhibit limited flexibility in predicting C_{rate}. ENR had the best performance in this category, with an overall RMSE of 19.3749 μm/year, CI of 0.5536, and R2 of 0.799. ENR increased prediction outcomes by 28.62 %, 16.66 %, and 8.32 % in terms of RMSE when compared to MLR, RR, and LR, respectively.
- EL-based predictive models outperformed regression models while maintaining physical integrity and predicting only positive C_{rate}. However, the DT model demonstrated a significant overfitting issue.
- XGB emerged as the top-performing model, achieving an impressive overall R^2 value of 0.982, an RMSE of 3.7805 μm/year, and a CI of 0.7254. The XGB outperformed the ADB, RD, and DT models in terms of R2 prediction, by 4.88 %, 4.42 %, and 17.07 %, respectively. Furthermore, the results are improved by 2.9 % compared to the best ML-model in the literature, proposed by Ben Seghier et al. [46].
- The SHAP analysis enhanced the interpretability of the XGB model's output and bolstered confidence in the reported results. The SHAP findings highlight the impact of CL^- on the C_{rate} as the factor with the highest influence during the XGB modeling. Additionally, all input variables displayed a proportional relationship with increasing C_{rate}, except for pH, which exhibited a disproportional impact.
- Finally, as no distinct vertical patterns of coloring were identified in the SHAP dependence scatter plots, it can be stated that the SHAP interaction effects of the analyzed features were negligible.

The consistent outcomes underscore the potential of EL approaches in addressing the intricate task of predictive modeling for the annual corrosion rate in suspension bridge main cables, especially when leveraging the XGB model. This model can be seamlessly incorporated into an interface to aid end users, such as operational engineers, in predicting and assessing corrosion. However, it is crucial to highlight the significance of data size and scale in any modeling endeavor employing ML models. This latter present the main current limitation for all data-driven methodologies. This means that the accuracy of the framework will be heavily dependent on the amount and quality of the data upon which it is implemented. Furthermore, the developed model can only be used within the explored design space covered by the range of values of the adopted parameters. Thus, results obtained from extrapolations to different values on the input parameters beyond the ones contained within the database used must be carefully interpreted. One strategy to circumvent this constraint is to use deep learning (DL) algorithms like Generative adversarial network (GAN) to generate more data based on expert and physical guidance from the field, which can then be combined with other DL techniques to produce more generalizable models in the future.

CRediT authorship contribution statement

Alejandro Jimenez Rios: Writing – original draft, Methodology, Investigation, Formal analysis. **Mohamed El Amine Ben Seghier:** Writing – original draft, Project administration, Methodology, Formal analysis, Data curation, Conceptualization. **Vagelis Plevris:** Writing – original draft, Validation, Supervision, Methodology. **Jian Dai:** Writing – original draft, Validation, Methodology.

Declaration of competing interest

The authors declare that they have no known competing financial interests or personal relationships that could have appeared to influence the work reported in this paper.

Data availability

Data will be made available on request.

Acknowledgments

This paper has received funding from the European Union's Horizon 2021 research and innovation programme under the Marie Sklodowska-Curie grant agreement No. 101066739 and 101061320. The APC was funded by Oslo Metropolitan University.

References

[1] A.S. Nowak, O. Iatsko, Are our bridges safe?. https://www.nae.edu/183130/Are-Our-Bridges-Safe, 2018.
[2] S.A. Mitoulis, et al., Bridge and transport network resilience - a perspective. Proceedings of the Institution of Civil Engineers: Bridge Engineering, 2021, https://doi.org/10.1680/jbren.21.00055.
[3] M. Abbas Majeed Al-Jaafari, Spatial variation of the bridge transport network in wasit governorate. https://ptgeo.org.pl/wp-content/uploads/2022/10/CG_2018_89_1-2_notatki-2.pdf, 2018.
[4] R. Cucuzza, et al., Vulnerability assessment and lifecycle analysis of an existing masonry arch bridge, Eng. Struct. 302 (2024) 117422, https://doi.org/10.1016/j.engstruct.2023.117422.
[5] B.S. Vishwanath, S. Banerjee, Capturing spatiotemporal progression of corrosion to estimate life-cycle seismic resilience of RC bridges, ASCE-ASME Journal of Risk and Uncertainty in Engineering Systems, Part A: Civ. Eng. 10 (1) (2024) 04023064, https://doi.org/10.1061/AJRUA6.RUENG-1109.
[6] O. Khandel, M. Soliman, Maintenance optimization for deteriorating bridges under uncertainty, in: Structures Congress 2018: Bridges, Transportation Structures, and Nonbuilding Structures - Selected Papers from the Structures Congress 2018, 2018, pp. 242–251, https://doi.org/10.1061/9780784481332.022.
[7] M. Hurt, S.D. Schrock, Highway bridge maintenance planning and scheduling, Highway Bridge Maintenance Planning and Scheduling 1–337 (2016), https://doi.org/10.1016/C2014-0-01037-4.
[8] BluePlan Engineering, 2019 Canada infrastructure report card. http://canadianinfrastructure.ca/downloads/canadian-infrastructure-report-card-2019.pdf, 2019.
[9] ASCE, 2021 report card for America's infrastructure. https://infrastructurereportcard.org/wp-content/uploads/2020/12/Bridges-2021.pdf, 2021.
[10] K. Gkoumas, et al., Research and innovation in bridge maintenance, inspection and monitoring. https://data.europa.eu/doi/10.2760/719505, 2019.
[11] R.Z. Alrousan, B.a.R. Alnemrawi, The behavior of alkali-silica reaction-damaged full-scale concrete bridge deck slabs reinforced with CFRP bars, Results in Engineering 16 (2022) 100651, https://doi.org/10.1016/j.rineng.2022.100651.
[12] A. Nettis, et al., On the use of satellite-based interferometry for structural monitoring of bridge portfolios, Procedia Struct. Integr. 44 (2023) 1996–2003, https://doi.org/10.1016/j.prostr.2023.01.255.
[13] A. Jiménez Rios, V. Plevris, M. Nogal, Bridge management through digital twin-based anomaly detection systems: a systematic review, Frontiers in Built Environment (2023), https://doi.org/10.3389/fbuil.2023.1176621.
[14] A. Jiménez Rios, V. Plevris, M. Nogal, Uncertainties in the synthetic data generation for the creation of bridge digital twins, in: 5th International Conference on Uncertainty Quantification in Computational Science and Engineering (UNCECOMP), 2023, https://doi.org/10.7712/120223.10323.20020. Athens, Greece.
[15] A. Jiménez Rios, V. Plevris, M. Nogal, Synthetic data generation for the creation of bridge digital twins what-if scenarios, in: 9th International Conference on Computational Methods in Structural Dynamics and Earthquake Engineering (COMPDYN), 2023, https://doi.org/10.7712/120123.10760.21262. Athens, Greece.
[16] K.H. Ostenfeld, Evolution of suspension bridges, Hormigon y Acero 70 (289) (2019) 103–113, https://doi.org/10.33586/hya.2019.2074.
[17] M. De Miranda, Long-span bridges, in: Innovative Bridge Design Handbook: Construction, Rehabilitation and Maintenance, 2021, pp. 463–508, https://doi.org/10.1016/B978-0-12-823550-8.00021-4.
[18] Y. Ding, et al., Aerodynamic stability evolution tendency of suspension bridges with spans from 1000 to 5000 m, Front. Struct. Civ. Eng. 17 (10) (2023) 1465–1476, https://doi.org/10.1007/s11709-023-0980-z.
[19] D. McFetrich, An Encyclopaedia of World Bridges, vol. 352, Pen & Sword Books, 2022. https://www.pen-and-sword.co.uk/An-Encyclopaedia-of-World-Bridges-Hardback/p/20379.
[20] T.R. Witcher, An icon at 80: the golden gate bridge, Civil Engineering Magazine 87 (6) (2017) 42–45, https://doi.org/10.1061/ciegag.0001205.
[21] Ö. Güzel, Çanakkale bridge – dream to reality, in: A. Ilki, D. Çavunt, Y.S. Çavunt (Eds.), Building for the Future: Durable, Sustainable, Resilient, Springer Nature Switzerland, Cham, 1915, pp. 27–46, https://doi.org/10.1007/978-3-031-32519-9_3, 2023.
[22] J.H. Gabra, A.K. Desai, Cable supported bridges for long to superlong spans, in: B. Kondraivendhan, C.D. Modhera, V. Matsagar (Eds.), Sustainable Building Materials and Construction, Springer Nature Singapore, Singapore, 2022, pp. 255–261, https://doi.org/10.1007/978-981-16-8496-8_33.

[23] K. Mahmoud, C. Gair, H. McDonald, Risk-based evaluation of main suspension cables of the forth road bridge in scotland, in: Risk-based Bridge Engineering - 10th NewYork City Bridge Conference, 2019, pp. 3–15, https://doi.org/10.1201/9780367815646-1, 2019.
[24] Y. Yuan, et al., Temporal and spatial variability of corrosion of high-strength steel wires within a bridge stay cable, Construct. Build. Mater. 308 (2021) 125108, https://doi.org/10.1016/j.conbuildmat.2021.125108.
[25] H. Li, et al., Study on failure mode and parameter influence of epoxy coating steel strand with the impact action, Case Stud. Constr. Mater. 18 (2023) e01951, https://doi.org/10.1016/j.cscm.2023.e01951.
[26] K. Dai, et al., Effect of outer rust layer on cathodic protection and corrosion behavior of high-strength wire hangers with sheath crack in marine rainfall environment, Case Stud. Constr. Mater. 18 (2023) e02043, https://doi.org/10.1016/j.cscm.2023.e02043.
[27] J.-W. Kim, J. Kim, S. Park, Cross-sectional loss quantification for main cable NDE based on the B-H loop measurement using a total flux sensor, J. Sens. 2019 (2019) 8014102, https://doi.org/10.1155/2019/8014102.
[28] X. Chen, M. Tang, Main cable opening inspection and bearing capacity evaluation of suspension bridge in service in Myanmar, Xinan Jiaotong Daxue Xuebao/Journal of Southwest Jiaotong University 57 (5) (2022) 1130–1137, https://doi.org/10.3969/j.issn.0258-2724.20200393.
[29] R. Betti, et al., Monitoring the structural health of main cables of suspension bridges, Journal of Civil Structural Health Monitoring 6 (3) (2016) 355–363, https://doi.org/10.1007/s13349-016-0165-8.
[30] J. Deeble Sloane Matthew, et al., Experimental analysis of a nondestructive corrosion monitoring system for main cables of suspension bridges, J. Bridge Eng. 18 (7) (2013) 653–662, https://doi.org/10.1061/(ASCE)BE.1943-5592.0000399.
[31] R. Singh, D. Prasad, Corrosion: basics, economic adverse effects, and its mitigation, in: Grafted Biopolymers as Corrosion Inhibitors, 2023, pp. 1–10, https://doi.org/10.1002/9781119881391.ch1.
[32] S. Li, et al., Atmospheric corrosion performance of wire rope sling in a sulfur dioxide-polluted environment, Adv. Mech. Eng. 9 (6) (2017) 1687814017707479, https://doi.org/10.1177/1687814017707479.
[33] D. Hu, et al., Experimental study on corrosion resistance of Zn–Al–Mg alloy coating of high-strength steel wires for bridge cables, Anti-corrosion Methods & Mater. 70 (6) (2023) 459–468, https://doi.org/10.1108/ACMM-07-2023-2858.
[34] K. Miyachi, et al., Experimental corrosion investigation of untreated suspension bridge main cables, in: IABSE Congress, New Delhi 2023: Engineering for Sustainable Development, Report, 2023, pp. 1191–1198, https://doi.org/10.2749/newdelhi.2023.1191.
[35] K. Suzumura, S.-i. Nakamura, Environmental factors affecting corrosion of galvanized steel wires, J. Mater. Civ. Eng. 16 (1) (2004) 1–7, https://doi.org/10.1061/(ASCE)0899-1561(2004)16:1(1).
[36] X. Han, M. Frangopol Dan, Impact of climate change on risk assessment and effective maintenance strategies for bridge networks subjected to corrosion, ASCE-ASME Journal of Risk and Uncertainty in Engineering Systems, Part A: Civ. Eng. 10 (1) (2024) 04023054, https://doi.org/10.1061/AJRUA6.RUENG-1059.
[37] H. Tian, et al., Probabilistic assessment of the safety of main cables for long-span suspension bridges considering corrosion effects, Adv. Civ. Eng. (2021), https://doi.org/10.1155/2021/6627762, 2021.
[38] C. Jin, X. Ru-cheng, Main cable safety factors assessment of long-span suspension bridges based on inverse reliability method, China J. Highw. Transp. 20 (1) (2007) 58–61.
[39] Y. Deng, Y. Liu, S. Chen, Long-term in-service monitoring and performance assessment of the main cables of long-span suspension bridges, Sensors 17 (6) (2017), https://doi.org/10.3390/s17061414.
[40] A. Valor, et al., Markov chain models for the stochastic modeling of pitting corrosion, Math. Probl Eng. 2013 (2013) 108386, https://doi.org/10.1155/2013/108386.
[41] J.L. Alamilla, E. Sosa, Stochastic modelling of corrosion damage propagation in active sites from field inspection data, Corrosion Sci. 50 (7) (2008) 1811–1819, https://doi.org/10.1016/j.corsci.2008.03.005.
[42] E. Karanci, R. Betti, Modeling corrosion in suspension bridge main cables. I: annual corrosion rate, J. Bridge Eng. 23 (6) (2018) 04018025, https://doi.org/10.1061/(ASCE)BE.1943-5592.0001233.
[43] E. Karanci, R. Betti, Modeling corrosion in suspension bridge main cables. II: long-term corrosion and remaining strength, J. Bridge Eng. 23 (6) (2018) 04018026, https://doi.org/10.1061/(ASCE)BE.1943-5592.0001234.
[44] J.-S. Chou, N.-T. Ngo, W.K. Chong, The use of artificial intelligence combiners for modeling steel pitting risk and corrosion rate, Eng. Appl. Artif. Intell. 65 (2017) 471–483, https://doi.org/10.1016/j.engappai.2016.09.008.
[45] H. Rezk, et al., Metaheuristic optimization algorithms for real-world electrical and civil engineering application: a review, Results in Engineering 23 (2024) 102437, https://doi.org/10.1016/j.rineng.2024.102437.
[46] M.E.A. Ben Seghier, et al., On the modeling of the annual corrosion rate in main cables of suspension bridges using combined soft computing model and a novel nature-inspired algorithm, Neural Comput. Appl. 33 (23) (2021) 15969–15985, https://doi.org/10.1007/s00521-021-06199-w.
[47] Y. Deng, et al., Predicting fatigue damage of highway suspension bridge hangers using weigh-in-motion data and machine learning, Structure and Infrastructure Engineering 17 (2) (2021) 233–248, https://doi.org/10.1080/15732479.2020.1734632.
[48] A.M. Hernández-Díaz, et al., Machine learning as alternative strategy for the numerical prediction of the shear response in reinforced and prestressed concrete beams, Results in Engineering 22 (2024) 102139, https://doi.org/10.1016/j.rineng.2024.102139.
[49] V. Yadav, et al., Artificial neural network an innovative approach in air pollutant prediction for environmental applications: a review, Results in Engineering 22 (2024) 102305, https://doi.org/10.1016/j.rineng.2024.102305.
[50] F. Harrou, et al., Enhancing road traffic flow prediction with improved deep learning using wavelet transforms, Results in Engineering 23 (2024) 102342, https://doi.org/10.1016/j.rineng.2024.102342.
[51] R.J. Jacques Molu, et al., Advancing short-term solar irradiance forecasting accuracy through a hybrid deep learning approach with Bayesian optimization, Results in Engineering 23 (2024) 102461, https://doi.org/10.1016/j.rineng.2024.102461.
[52] H. Li, S. Sen, L. Khazanovich, A scalable adaptive sampling approach for surrogate modeling of rigid pavements using machine learning, Results in Engineering (2024) 102483, https://doi.org/10.1016/j.rineng.2024.102483.
[53] L. Stagi, et al., Enhancing the damage detection and classification of unknown classes with a hybrid supervised–unsupervised approach, Infrastructures 9 (3) (2024), https://doi.org/10.3390/infrastructures9030040.
[54] Chencho, et al., Structural damage classification of large-scale bridges using convolutional neural networks and time domain responses, J. Perform. Constr. Facil. 38 (4) (2024) 04024019, https://doi.org/10.1061/JPCFEV.CFENG-4676.
[55] S. Lundberg, S.-I. Lee, A unified approach to interpreting model predictions, arXiv [cs.AI] (2017), https://doi.org/10.48550/arXiv.1705.07874.
[56] D.C. Montgomery, G.C. Runger, Applied Statistics and Probability for Engineers, Wiley, 2018, p. 720. https://www.wiley.com/en-us/Applied+Statistics+and+Probability+for+Engineers%2C+7th+Edition-p-9781119400363.
[57] R.V. McCarthy, M.M. McCarthy, W. Ceccucci, Predictive models using regression, in: R.V. McCarthy, M.M. McCarthy, W. Ceccucci (Eds.), Applying Predictive Analytics: Finding Value in Data, Springer International Publishing, Cham, 2022, pp. 87–121, https://doi.org/10.1007/978-3-030-83070-0_4, 10.1007/978-3-030-83070-0_4.
[58] C. Hans, Elastic Net regression modeling with the orthant normal prior, J. Am. Stat. Assoc. 106 (496) (2011) 1383–1393, https://doi.org/10.1198/jasa.2011.tm09241.
[59] D.C. Montgomery, E.A. Peck, G.G. Vining, Introduction to Linear Regression Analysis, Wiley, 2021, p. 704. https://www.wiley.com/en-us/Introduction+to+Linear+Regression+Analysis,+6th+Edition-p-9781119578727.
[60] W.N. van Wieringen, Lecture notes on ridge regression, arXiv [stat.ME], https://doi.org/10.48550/arXiv.1509.09169, 2023.
[61] T. Hastie, R. Tibshirani, M. Wainwright, Statistical Learning with Sparsity the Lasso and Generalizations, vol. 368, Routledge Taylor & Francis Group, 2015. https://www.routledge.com/Statistical-Learning-with-Sparsity-The-Lasso-and-Generalizations/Hastie-Wainwright-Tibshirani/p/book/9780367738334?gclid=CjwKCAiAvoqsBhB9EiwA9XTWGbojiAjNrxR_qS4rKjzA-YrVSEOCUYTcDfdS6vYtOjrdC06kQyX3jhoCdrQQAvD_BwE.
[62] M.E.A. Ben Seghier, D. Höche, M. Zheludkevich, Prediction of the internal corrosion rate for oil and gas pipeline: implementation of ensemble learning techniques, J. Nat. Gas Sci. Eng. 99 (2022) 104425, https://doi.org/10.1016/j.jngse.2022.104425.
[63] X. Ma, Using Classification And Regression Trees: A Practical Primer, Information Age Publishing, 2018. https://www.infoagepub.com/products/Using-Classification-and-Regression-Trees.
[64] Z.-H. Zhou, Ensemble learning, in: Z.-H. Zhou (Ed.), Machine Learning, Springer Singapore, Singapore, 2021, pp. 181–210, https://doi.org/10.1007/978-981-15-1967-3_8.
[65] M.E.A. Ben Seghier, V. Plevris, G. Solorzano, Random forest-based algorithms for accurate evaluation of ultimate bending capacity of steel tubes, Structures 44 (2022) 261–273, https://doi.org/10.1016/j.istruc.2022.08.007.
[66] L. Breiman, Random forests, Mach. Learn. 45 (1) (2001) 5–32, https://doi.org/10.1023/A:1010933404324.
[67] A.R. Ghanizadeh, A. Tavana Amlashi, S. Dessouky, A novel hybrid adaptive boosting approach for evaluating properties of sustainable materials: a case of concrete containing waste foundry sand, J. Build. Eng. 72 (2023) 106595, https://doi.org/10.1016/j.jobe.2023.106595.
[68] G.-Q. Liang, et al., Fatigue life prediction of concrete under cyclic compression based on gradient boosting regression tree, Mater. Struct. 56 (9) (2023) 172, https://doi.org/10.1617/s11527-023-02262-1.
[69] C. Wang, W. Xiao, J. Liu, Developing an improved extreme gradient boosting model for predicting the international roughness index of rigid pavement, Construct. Build. Mater. 408 (2023) 133523, https://doi.org/10.1016/j.conbuildmat.2023.133523.
[70] M.E.A. Ben Seghier, et al., An intelligent framework for forecasting and investigating corrosion in marine conditions using time sensor data, npj Mater. Degrad. 7 (1) (2023) 91, https://doi.org/10.1038/s41529-023-00404-y.
[71] M.E.A. Ben Seghier, et al., Modeling the nonlinear behavior of ACC for SCFST columns using experimental-data and a novel evolutionary-algorithm, Structures 30 (2021) 692–709, https://doi.org/10.1016/j.istruc.2021.01.036.
[72] M.E.A. Ben Seghier, et al., Simulation of the ultimate conditions of fibre-reinforced polymer confined concrete using hybrid intelligence models, Eng. Fail. Anal. 128 (2021) 105605, https://doi.org/10.1016/j.engfailanal.2021.105605.
[73] K.E. Taylor, Summarizing multiple aspects of model performance in a single diagram, J. Geophys. Res. Atmos. 106 (D7) (2001) 7183–7192, https://doi.org/10.1029/2000JD900719.
[74] S. Permeh, K. Lau, Corrosion of galvanized steel in alkaline solution associated with sulfate and chloride ions, Construct. Build. Mater. 392 (2023) 131889, https://doi.org/10.1016/j.conbuildmat.2023.131889.